European Journal of Mechanics B/Fluids 29 (2010) 269–277

Contents lists available at ScienceDirect

European Journal of Mechanics B/Fluids

journal homepage: www.elsevier.com/locate/ejmflu

An experimental study of a radial wall jet formed by the normal impingement of a round synthetic jet

Gopi Krishnan, Kamran Mohseni *

Department of Aerospace Engineering Sciences, 429 UCB, University of Colorado, Boulder, CO 80309, USA

ARTICLE INFO

Article history:
Received 2 May 2009
Received in revised form
8 February 2010
Accepted 4 March 2010
Available online 23 March 2010

Keywords:
Synthetic jet
Wall jet
Impingement

ABSTRACT

The flow field of a radial wall jet created by the impingement of a round synthetic jet normal to a flat surface was characterized using hot-wire anemometry. In the synthetic wall jets the width of the outer layer was observed to increase linearly with the radial distance along the wall, while the local maximum velocity varied inversely. The synthetic wall jet exhibits self-similar behavior as distinguished by the collapse of the mean and rms velocity profiles when normalized by the outer layer scaling variables. Increasing the actuator driving amplitude at a fixed frequency (i) increased the growth rate of the outer layer, and (ii) decreased the decay rate of the local velocity maximum. The flow field of the synthetic wall jet was dominated by vortical structures associated with the actuator driving frequency, and harmonics connected with the interaction of the produced vortex structures. For the actuator conditions investigated, neither the classical laminar nor fully turbulent analytical solutions for continuous wall jets were amenable to modeling the synthetic wall jet profile due to the transitional and unsteady nature of the synthetic wall jet.

1. Introduction

A synthetic jet, or a zero net mass flux (ZNMF) jet, is a type of fully periodic jet that results from the formation and interaction of vortex rings or pairs [1]. A common method of generating a synthetic jet in a single-phase fluid is the application of a threshold periodic pressure gradient across an orifice. This affects the cyclic inception of a shear layer at the orifice edge, which in turn, rolls up into a vortex ring that travels downstream due to its self-induced velocity. Fig. 1 shows a schematic of the suction and ejection strokes that constitute a cycle in this synthesis. In this fashion, a train of vortex rings moving away from the orifice occurs, whereupon the coherent structures then interact, coalesce, and break down in a transition towards a turbulent jet directed downstream. This operational principle allows for a synthetic jet to be synthesized entirely from the surrounding medium, while at the same time imparting a net momentum flux to the external flow. In addition, the ability to influence the surrounding medium at a variety of scales makes the synthetic jet attractive to a number of applications [2].

One such application where synthetic jets have been shown to be advantageous is that in cooling of electronic components [3–8]. A configuration commonly employed in the above application is that where a synthetic jet impinges normally upon a surface. This mechanism is shown to enhance the heat transfer characteristics due to the following properties. First, the impingement of the primary and secondary vortical structures on the heated surface increases the wall normal velocity fluctuations, thereby increasing the momentum transfer in the layers closest to the wall which as a consequence increases the heat transfer rate [9,10]. Second, the synthetic jet entrains more fluid when compared to an equivalent continuous jet, which increases the volume of fluid impinging upon a surface augmenting the heat transfer capacity. Upon impingement the ensuing flow that is nominally parallel to the surface is termed a radial wall jet, and bears relevance to this study. With the heat transfer characteristics in this region being dependent on the both hydrodynamic and thermal flow fields, this paper attempts to address the former. In this regard, this study experimentally characterizes a synthetic jet-induced wall jet and examines the effect of the actuator driving amplitude on the mean flow field.

Fig. 2, presents the evolution of the flow of a synthetic jet impinging normally upon a wall where the flow may be divided into four regions. The region in the near field of the orifice is typified by the presence of discrete coherent vortex rings and fully periodic flow. Further downstream the vortex rings begin to interact and breakdown, reducing their coherence as they transition towards a free turbulent jet directed normal to the wall. The synthetic free jet exhibits similarities to continuous turbulent free jets in their self-similar behavior, while demonstrating an enhanced spreading rate [1]. As the jet approaches the wall the axial velocity decreases

* Corresponding author.
E-mail address: mohseni@colorado.edu (K. Mohseni).

0997-7546/$ – see front matter © 2010 Elsevier Masson SAS. All rights reserved.
doi:10.1016/j.euromechflu.2010.03.001

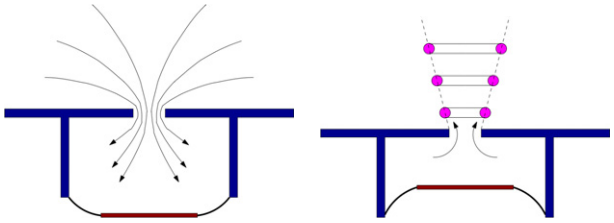

(a) Suction. (b) Ejection.

Fig. 1. Schematic of the synthetic jet operation displaying the suction and ejection strokes.

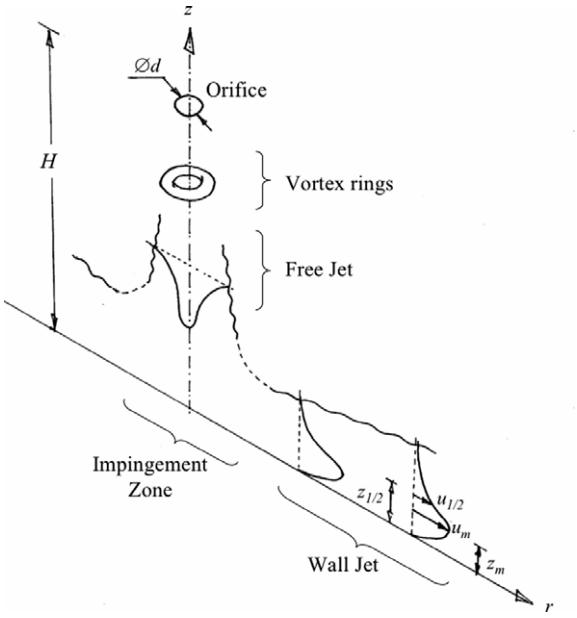

Fig. 2. Schematic of the evolution of the flow due to the normal impingement of a round synthetic jet upon a wall. Shown, are vortex rings in the near field of the orifice, and mean velocity profiles of both, free and wall jets in the far field.

rapidly with the static pressure increasing on account of the presence of a stagnation point at the wall [11]. The jet then is directed radially outwards along the wall where the flow is temporarily accelerated on account of the local pressure gradient [11]. Away from the immediate region of impingement the flow develops into a fully developed wall jet where both a free and solid boundary exists.

Wall jets have been described as a boundary layer flow to which momentum has been added upstream, such that a local velocity maximum exists in the shear layer that exceeds that of the free stream [12]. As seen in the wall jet region in Fig. 2, two regions may be distinguished. The region closer to the wall where the velocity increases from zero at the wall to a local maximum (u_m) is considered the inner layer ($0 < z < z_m$), while the region beyond this velocity maximum, where the velocity decays to the free stream velocity is regarded as the outer layer ($z_m < z < \infty$). While the inner and outer layer bear some resemblance to boundary layers and free jets respectively, it is the dissimilar nature of the two shear layers and their interaction that gives rise to the singular characteristics of a wall jet [12]. For instance, the maximum shear stress in the wall jet does not occur at the location where the velocity gradient is zero (z_m) but is displaced closer to the wall. Further, the spreading rate of the outer layer is observed to be less than that of a free jet. However, the characteristic length and velocity scales describing the self-similar nature of the individual shear layers have been shown to apply in the wall jet. However, dissimilar characteristic length and velocity scales present in each layer, preclude the complete self-similar description of the entire wall jet using a single scaling [13,14].

In terms of the analytical modeling of the mean velocity profiles in steady wall jets, the laminar configuration has been shown to yield a closed-form solution of the self-similar kind [15,16] where experiments [17] have validated the solution. This analytical result is extended to turbulent wall jets [16] by modeling the inner and outer regions of the flow separately and matching the solutions at the location of the local maximum velocity. The routine employs an eddy viscosity approximation that varies in accordance to the region, resulting in a velocity profile containing a single empirical parameter that is reflective of the turbulent nature of the flow. Once again the turbulent model shows close agreement with experimental results [18,19]. Now, wall jets subject to forcing have been shown to be additionally dependent on the excitation frequency and amplitude. In the case of forced laminar wall jets even small amplitude excitations at particular frequencies significantly affect the mean velocity field [20,21]. In forced turbulent jets the effect of external excitation has been shown to nominally increase the spreading rate [22,23]. However, beyond a critical Reynolds number of $\sim$3000, the impact of excitation on the self-similar mean velocity profiles are marginal [22].

For the problem at hand, several parameters that may influence the flow structure are evident. They include amongst others, the geometry of the actuator, the actuation parameters, and the orifice-to-wall height. With the prevalent flow phenomena in each of the regions differing, the controllable parameters will influence each zone in a disparate manner. For example, the evolution of the vortex rings in the near field is dependent on the actuation parameters that include the driving frequency and amplitude [24]. Furthermore the actuation parameters influence the spreading and subsequent entrainment rate of the free synthetic jet [1]. In the impingement region, the nozzle-to-wall distance is additionally seen to effect the generation of secondary vortical structures upon impact [25]. With the wall jet being a consequence of the preceding regions, it seems to reason that the aforementioned factors play a role in the development of the wall jet. This is justified by work that goes to show that the heat transfer rate due to synthetic jet impingement does indeed vary with the above parameters [7,8].

In this paper the geometry of the actuator and orifice-to-wall distance (H/d) are fixed, while the amplitude of the sinusoidal signal that drives the piezoelectric membrane is varied at a fixed frequency. It is known that two non-dimensional variables; namely, the stroke ratio (L/d) and Reynolds number (Re_{U_o}), are the primary actuator parameters that influence free synthetic jets [1]. The stroke ratio is representative of the length of the slug of fluid ejected from the orifice during the expulsion stroke and may also be interpreted as an inverse Strouhal number [26]. Further, the Reynolds number embodies the velocity of this ejected slug where explicit definitions are given later in the paper. In keeping the frequency constant and varying the driving voltage, both the Reynolds number and stroke ratio do vary. However unlike free synthetic jets where the Reynolds number does not significantly influence the development of the jet [27], it is not possible to presuppose that for a wall jet as it has been observed that the heat transfer capacity in impinging synthetic jets is impacted by actuator frequency and jet Reynolds number [7]. Using a piezoelectric diaphragm as a driver as is the case here, gives rise to the coupling between frequency and deflection and consequently stroke ratio and Reynolds number. Thus the range over which the stroke ratio and Reynolds number may independently vary is limited. Consequently in this preliminary study the impact of the Reynolds number and stroke ratio are not independently investigated.

With previous work focusing on the impingement region of synthetic jets, the contribution of this study is to characterize the

wall jet region. So it is in this vein that we seek to answer the following questions: (i) what are similarities between synthetic and continuous wall jets, (ii) how do the two differ, (iii) what effect does the actuator driving amplitude have on the wall jet and finally, (iv) are the classic solutions to steady wall jets applicable to modeling synthetic wall jets.

This study is a continuation of our investigation in modeling and experimentation on axi-symmetric and two-dimensional synthetic jets in quiescent environment [28,29]. Extension of these works to wall jet is presented here. Synthetic jets in co-flow and cross-flow are the subject of our future publications [30].

This paper is outlined as follows: Section 2, briefly outlines the models of the velocity profiles of steady continuous wall jets and their possible applicability to synthetic wall jets, and then defines critical actuator parameters. The experimental setup for the measurement of the velocity field and diaphragm deflection is then described in Section 3. After which, the results are presented and discussed in Section 4. Concluding remarks are presented in Section 5.

2. Analytical models

2.1. Time average flow field

In this section three established models for the mean velocity of a continuous steady wall jet are outlined and their possible applicability towards synthetic wall jets discussed. The first is a closed form solution to a laminar wall jet. The second is a semi-empirical solution to a fully turbulent wall jet, and the third is a purely empirical solution that combines the form of the velocity profiles of a turbulent boundary layer and a free shear layer.

2.1.1. Laminar closed form model

The classic solution for a laminar wall jet [15,16] is briefly outlined here. For a radial, steady, incompressible, laminar wall jet, it is possible to describe the flow using boundary layer approximations. The governing equations may be expressed as

$$u\frac{\partial u}{\partial r}+v\frac{\partial u}{\partial z}=\nu\frac{\partial^2 u}{\partial z^2},\quad \text{and}\quad \frac{\partial (ru)}{\partial r}+\frac{\partial (rv)}{\partial z}=0, \tag{1}$$

with boundary conditions

$$\text{at } z=0;\qquad u=v=0,\quad \text{and}\quad z\to\infty;\qquad u\to 0, \tag{2}$$

where r and z are the radial and axial coordinate respectively, with u and v being the radial and axial velocity components respectively, and ν being the kinematic viscosity. Considering U and δ as characteristic velocity and length scales, a similarity solution of the form $u/U=f'(r/\delta)$ is sought. The similarity variable is expressed as $\eta=\eta(r/\delta)$ and the characteristic velocity and length scales are proposed to vary as $U\propto r^a$, and $\delta\propto r^b$ respectively. Through the use of (i) a stream function formulation, (ii) the conservation of exterior momentum flux, and (iii) the given boundary conditions, the self-similar equation is written as

$$f'''+ff''+2f'^2=0, \tag{3}$$

with boundary conditions $f(0)=f'(0)=0$ and $f''(\infty)=0$. An analytical closed form solution to the above exists and is displayed in Fig. 3.

The possible applicability of the laminar solution towards describing a synthetic wall jet is questionable on two grounds. First, the synthetic wall jet is unlikely to be laminar due to the vigorous interaction of vortical structures in the free jet, and the added impact and spreading at the wall. Second, continuous laminar wall jets upon excitation show significant deviation from the closed form solution described above, where forcing results in the widening of the boundary layer [20,21]. This effect was attributed to the dominance of the outer layer vortex mixing process, resulting in fluid being transported away from the wall and the subsequent thickening of the inner layer. With the synthetic wall jet being fully pulsed, similar behavior in terms of the lift off away from the wall may be anticipated. With the laminar jet solution not able to account for the additional momentum transfer due to vortical mixing, it is probably incapable of describing the synthetic wall jet as will be seen later.

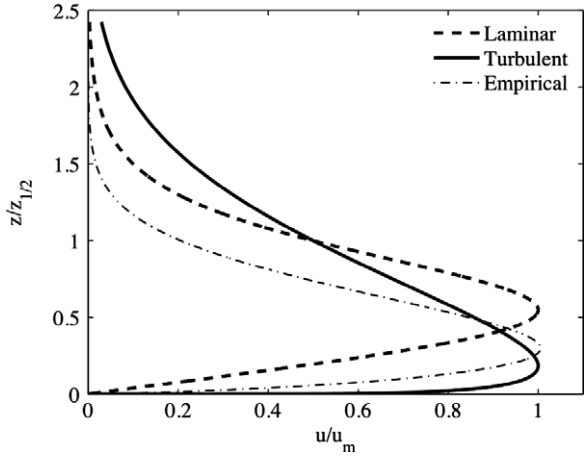

Fig. 3. Representative velocity profiles of the closed form laminar, semi-empirical turbulent, and empirical wall jet solutions. The dashed line represents the classic laminar wall jet solution, the solid line shows a turbulent jet solution for $\alpha=1.4$, while the dash-dot line shows an intermediate profile that is later seen to represent the synthetic wall jet for the parameters employed.

2.1.2. Turbulent semi-empirical model

For a fully turbulent steady wall jet, a semi-empirical model of the mean velocity profiles exists [16]. Boundary layer equations (Eq. (1)) form the basis of the analysis along with an eddy viscosity approximation used in replacing the kinematic viscosity. The flow is divided into two regions. In the inner layer the eddy viscosity is assumed to vary as $\varepsilon\propto z^{6/7}$, much like a Blasius boundary layer in a pipe, while in the outer layer it remains constant $\varepsilon=\varepsilon_o$, in the manner of a free turbulent jet. In addition to the first two assumptions stated above for the laminar case, the use of (i) the assumed variation in the eddy viscosity within the respective regions and, (ii) a method of matching solutions of the inner and outer layer (see [16] for a complete derivation), results in a self-similar equation in the outer layer (f_o) written as

$$f_o'''+f_of_o''+\alpha f_o'^2=0, \tag{4}$$

and the inner layer (f_i) as

$$\frac{\partial}{\partial\eta}(Af_i'^6f_i'')+f_if_i''+\alpha f_i'^2=0, \tag{5}$$

with boundary conditions;

$$\begin{aligned}&\eta\to 0;\qquad f_i'\eta^{-1/7}\to C,\qquad f_o(\infty)=0,\qquad \eta=\eta_m;\\ &f_o=f_i,\qquad f_o'=f_i',\qquad f_o''=f_i''.\end{aligned} \tag{6}$$

The above equations are numerically integrated to obtain the inner and outer solution, where A and α are constants that emerge from the analysis.

Previous work [13] has shown that the jet Reynolds number does affect the velocity decay and spreading rate in a turbulent wall jet. However, beyond a certain threshold jet Reynolds number the self-similar collapse of the mean velocity profiles do not differ and are approximated well with an analytical solution corresponding

to $\alpha = 1.3$–1.4. Fig. 3 shows the turbulent solution for $\alpha = 1.4$. In moving from the laminar to turbulent solution, an increase in the velocity gradient in the inner layer is seen, as is the reduction of the location of the local maximum velocity. This may be attributed to the change in momentum transfer mechanism from viscous diffusion to turbulent mixing. The outer layer tends to spread away from the wall much like a free shear layer, and the inner layer develops a steeper gradient akin to the way a boundary layer reacts to the transition from laminar to turbulent flow.

As with a laminar forced wall jet, the effect of external excitation upon a turbulent wall jet is to increase the outer spreading rate and reduce the velocity gradient near the wall [22]. In contrast to the excited laminar jet, excitation has a marginal effect on the self-similar collapse of the mean velocity profiles in a turbulent wall jet. This suggests that the inner and outer layers move away from the wall at much the same rate when subject to the external forcing, quite unlike that seen in laminar forced jets. This fact allows for the semi-empirical steady turbulent solution described above to adequately model a forced turbulent wall jet. It should be noted however that the amplitude of external excitation was limited to 20% in the above mentioned studies. This being said, the extension of the use of the steady turbulent wall jet solution to model a synthetic wall jet relies on (i) the Reynolds number of the synthetic jet flow being high enough so that flow is fully turbulent and (ii) the lack of dependence of the scaled velocity profiles on external forcing continuing to apply at much higher excitations as are seen in synthetic wall jets.

2.1.3. Empirical model

As explained above, under the conditions that either (i) the purely laminar or fully turbulent assumptions do not apply, or (ii) the unsteady nature of the jet results in significantly influencing the scaled mean velocity profiles, the above laminar and turbulent formulations may not be pertinent. An alternative approach is based on fitting a description to the velocity profile that is derived informally from the individual forms of the velocity profiles in boundary layer and shear layer. One such function commonly used is given by [31]

$$\frac{u}{U_m} = A\left(\frac{z}{z_{1/2}}\right)^{1/n}\left(1 - \operatorname{erf}\left(B\left(\frac{z}{z_{1/2}}\right)\right)\right), \tag{7}$$

where A, B and n are constants to be determined by a fitting procedure. As mentioned earlier, the wall jet possesses some characteristics akin to a free jet in the outer layer, and a boundary layer in the inner layer. Thus Eq. (7) may be considered the product of a power law and error function, where the power law dominates near the wall and the error function dominates in the outer layer. While the function has no rigorous theoretical basis, it provides a simple alternative to modeling the velocity profiles since at both intermediate Reynolds number flow and externally excited flows no fundamental theory exists to describe the wall jet. A representative profile intermediate between a steady laminar wall jet and fully turbulent wall jet is shown in Fig. 3. It is anticipated that the scaled synthetic wall jet profiles for the present actuator conditions will lie between the two extremes and be described using this purely empirical profile.

Hitherto, models for the external flow field of wall jets have been presented. With continuous steady jets the critical non-dimensional parameter of interest is a Reynolds number (Re) based on the steady exit bulk velocity. However, the upshot of the fully periodic nature of synthetic jets is (i) that a steady bulk exit velocity does not exist and hence a suitable average velocity needs to be defined, and (ii) some way of characterizing the oscillatory nature of the flow is required. These questions are addressed in the next section.

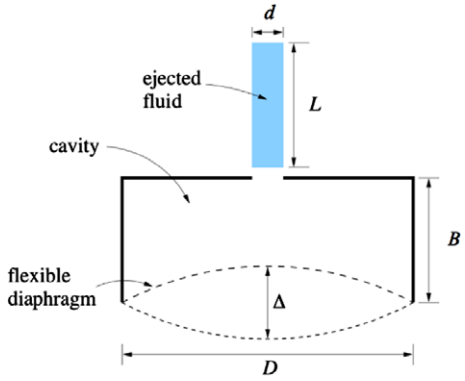

Fig. 4. Schematic of the actuator model, where the volume of fluid displaced by the diaphragm is ejected through the orifice in the form of a slug.

2.2. Actuator model

As mentioned earlier a non-dimensional stroke ratio, L/d and Reynolds number, Re have been established as key actuator operational parameters that influence a synthetic jet [1]. For the cavity-diaphragm setup used in this experiment they are obtained from an incompressible flow model, where it is assumed that the volume displaced by the membrane is equal to the volume ejected from the orifice (Fig. 4). To obtain the volume displaced by the membrane the shape of the deflected membrane and the central amplitude are required. The shape is obtained from the classical theory of plates [32], while the center amplitude is measured using a laser sensor. With the ejected volume approximated as a cylindrical slug of fluid with the same cross section as the exit orifice, the conservation of volume is written as

$$\alpha\frac{\pi D^2}{4}\Delta = \frac{\pi d^2}{4}L, \tag{8}$$

where α is the fraction of the volume displaced by an imaginary piston undergoing a peak to peak deflection of Δ, and is expressed as

$$\alpha = \frac{2\pi\int_0^{D/2} y(r)r\,\mathrm{d}r}{\frac{\pi D^2}{4}\Delta}, \tag{9}$$

where $y(r)$ is the deflection profile of the diaphragm. In assuming that the shape of the membrane is modeled by the static deflection of the circular membrane clamped on the edge subject to a uniform load, the deflection profile is written as

$$y(r) = \frac{\Delta}{2}\left[1 - \frac{r^2}{R^2} + \frac{2r^2}{R^2}\ln\left(\frac{r}{R}\right)\right], \tag{10}$$

where r is the radial coordinate and R is the radius of the membrane. The above deflection profile results in an α of 0.25. The non-dimensional stroke ratio is then determined to be

$$\frac{L}{d} = \alpha\Delta\frac{D^2}{d^3}. \tag{11}$$

The periodic nature of synthetic jets allows for the velocity scales to be defined based on either volume or momentum flux [33]. If based on volume flux the velocity scale is given as $U_o = \frac{L}{T} = fL$, and if based on momentum flux it is given as $U_o = \sqrt{2}\frac{L}{T} = \sqrt{2}fL$. It is more appropriate to use the velocity scale based on momentum flux here as the self-similar jet solutions employed in this study define equivalent jets based on the same momentum flux and not mass flux. Consequently, the Reynolds number is defined as

$$Re = \frac{U_o d}{\nu} = \frac{\sqrt{2}fLd}{\nu} = \frac{\sqrt{2}f\alpha\Delta D^2}{\nu d}. \tag{12}$$

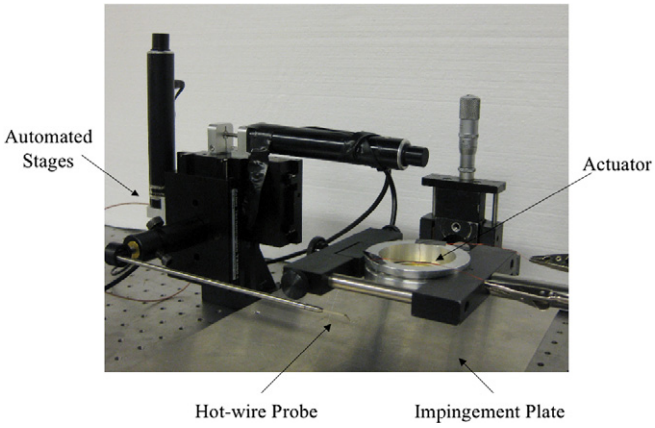

Fig. 5. The experimental setup used to measure the velocity field in the radial wall jet.

The Reynolds number is explicitly seen to vary with both membrane driving frequency and amplitude, with the stroke ratio appearing to be independent of frequency. This independence of stroke ratio on frequency is not accurate as the use of a piezoelectric diaphragm as a driver gives rise to the coupling between frequency and deflection, and consequently stroke ratio. However, for purposes of calculating the jet parameters the model serves the purpose. In summary, Eqs. (11) and (12) express the dependency of the critical actuator parameters on the diaphragm driving frequency and deflection amplitude.

The experimental setup used to characterize the wall jet flow field and the diaphragm deflection are described next.

3. Experimental setup

3.1. Wall jet flow field

The experimental setup to characterize the flow field of the synthetic wall jet is shown in Fig. 5. It consisted of a synthetic jet actuator, computer controlled stages, a boundary layer hot-wire probe and an impingement plate, all of which were placed in a large Plexiglas enclosure (not shown).

The actuator (Fig. 6) was comprised of a circular piezoelectric membrane sandwiched between two circular aluminum elements, which when screwed together formed a cavity with an orifice on one end and a flexible membrane on the other. They were three components in the design that were identified as being critical to the repeatable and reliable operation of the synthetic jet actuator. The first was the construction of the driving mechanism itself. The bonding between the piezoelectric material and the brass shim influenced the structural properties of the driver. As the facilities to properly bond the piezoelectric disc to the brass shim were not available, a commercially available alternative was used. It was observed through dynamic deflection measurements that the variability in bonding in the commercially available piezoelectric membranes, resulted in minimal variation within runs of a single membrane, as well as that between different membranes. The second critical area was the method to affix the membrane to the cavity. An initial attempt to glue the membrane to the cavity resulted in significant variation in the performance of the actuator. Thus, clamping the membrane between two aluminum elements by means of screwing them together resulted in repeatable measurements. The third area of focus was the finish of the orifice. Small nicks and other deviations from the cylindrical design of the orifice were observed to vary the characteristics of the external flow field. With the actuator fabricated using a CNC lathe, upon assembly, the orifice was inspected for any irregularities. These

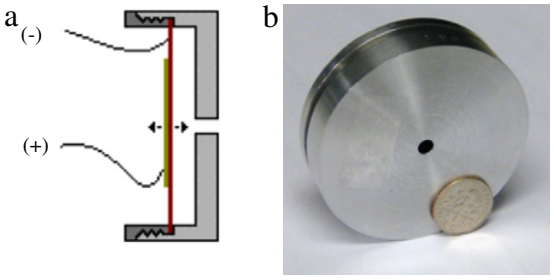

Fig. 6. A round synthetic jet actuator: (a) a schematic (b) an actuator alongside a dime provided for scale.

Table 1
Test matrix for actuator 1, displaying the driving frequency (f), voltage (V_d) and corresponding non-dimensional actuator parameters (L/d, Re).

Case #	f	V_d	L/d	Re
1	570	20	1.5	1632
2	570	30	1.8	1958
3	570	40	2.1	2285

design considerations then resulted in repeatable and reliable synthetic jet formation.

The dimensions of the orifice diameter (d) and depth (b) were 4.5 mm and 0.5 mm respectively, while the cavity diameter (D) and depth (B) were 40 mm and 3.4 mm respectively. A sinusoidal input voltage drove the piezoelectric membrane, the frequency and amplitude of which were controllable. In this paper the driving frequency (f_1) was fixed at 570 Hz which maximized the downstream mean velocity, while the driving amplitude (V_d) was varied from 20 V to 40 V. The test matrix along with the relevant non-dimensional parameters are summarized in Table 1.

The velocity measurements were made using a hot-wire anemometry system along with a single boundary layer wire probe (Dantec Dynamics 55P15). The probe consisted of offset prongs that were aligned such that they were parallel to the radial direction. The hot-wire system was calibrated in an iterative procedure [34] with a fourth order polynomial curve used to convert voltage to velocity. The signal acquired at 50 kHz was fed through a low pass filter with a cutoff frequency of 10 kHz. The hot-wire probe was affixed to a holder positioned on two computer control stages capable of traversing the vertical plane with a sensitivity of 1 μm. In traversing the flow field the stages were moved in discrete intervals normal and parallel to the impingement plate, where at each location the flow was sampled for 10 s. The radial and axial extent over which the measurements were made were $2 < r/d < 6$, and $0.1 < z/d < 2$ respectively. An aluminum plate served as the impingement surface for the synthetic jet, where the orifice-to-wall distance (H/d) was fixed at 9. This distance was selected as the synthetic free jet was observed to be fully developed prior to impingement at this distance.

The sources of uncertainty in the hot-wire anemometer were primary attributed to calibration, data reduction, and positioning. The calibration process constituted the largest source of uncertainty. At less than 10 L/min the uncertainty in flow rate was 20%, corresponding to an uncertainty of 20% at velocities less than 1 m/s. At higher flow rates and velocities, a more steady flow was readily achieved resulting in a uncertainty of about 2% at velocities greater than 1 m/s. The uncertainty in the positioning of the probe perpendicular to the axis of the jet was estimated to be around $\pm 2^\circ$, resulting in an associated error of 0.06%. The error associated with the DAQ is 0.05% and that with the curve fit less than 0.5%. With the uncertainties weighted equally and using a sum of squares method, a typical uncertainty at a velocity greater than 1 m/s was $\approx$2%.

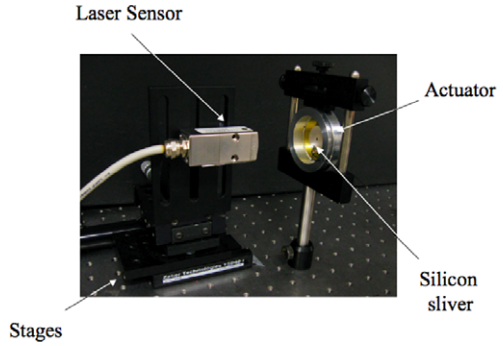

Fig. 7. The experimental setup used to obtain the deflection of the oscillating diaphragm.

3.2. Diaphragm deflection

The setup to measure the centerline deflection (Δ) of the piezoelectric membrane consists of a laser sensor, a movable stage, and a small sliver of silicon affixed to the center of the piezoelectric membrane while it is housed in the actuator (Fig. 7). The principle of operation of the laser sensor is as follows: A laser beam generated by the sensor is incident upon a reflective surface (the piece of silicon serves this purpose) on the diaphragm. The reflected beam returns though the same sensor opening whereupon it passes though an optical system and is projected on photo diodes. As the target moves back and forth, the position of the reflected beam translates on the photo diode surface where this translation is correlated to the motion of the target through calibration. The calibration of the sensor was conducted as such: With the sensor attached to a movable automated stage and the diaphragm fixed in a particular location, the laser was moved in increments of 1 μm towards the diaphragm with the signal response measured at each location. This non-linear displacement-response curve then serves as the calibration curve. To make measurements the laser is positioned at the location that allows for the largest sensitivity over the measurable range. To estimate the overall measurement accuracy of the laser the uncertainties associated with stage position, sensor resolution, calibration and experimental repeatability were taken into account. For a typical value the total combined uncertainty was estimated to be ± 1 μm. The measurements of the dynamic response of the diaphragm result in the central deflection of the membrane (Δ) and the frequency of diaphragm oscillation f. Direct measurement of the diaphragm oscillation grantees removes the need for any ad-hoc estimation of these parameters.

4. Results and discussion

In order to verify the validity of the experimental method, the flow field of a continuous turbulent jet impinging upon the wall was initially studied. A jet with average velocity (U_j) of 62 m/s issuing from an orifice of diameter (d) 5.8 mm was made to impinge normally upon a wall 10 diameters away from the exit. The jet Reynolds number was calculated to 24,294. The mean velocity profiles in the resulting wall jet region were measured with the normalized profile shown in Fig. 8. The profiles indeed collapse, where an analytical turbulent solution (Section 2) with $\alpha = 1.42$ agrees well with the experimental data.

With the experimental setup verified the synthetic wall jet is studied next. The mean velocity profiles for case 3 are presented in Fig. 9. The development of the wall jet is evidenced by the decrease in the local maximum velocity and increase in the width as the jet progresses radially outwards. The local velocity maxima in the profiles make it possible to discriminate an outer and inner layer.

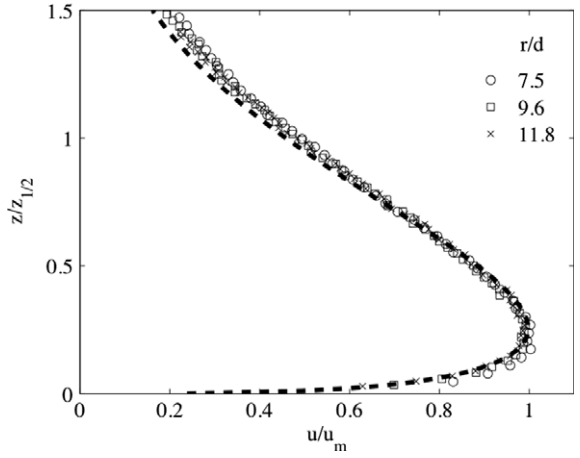

Fig. 8. The normalized mean velocity profile of a wall jet induced by the normal impingement of a continuous jet. The dashed line represents a semi-empirical turbulent solution.

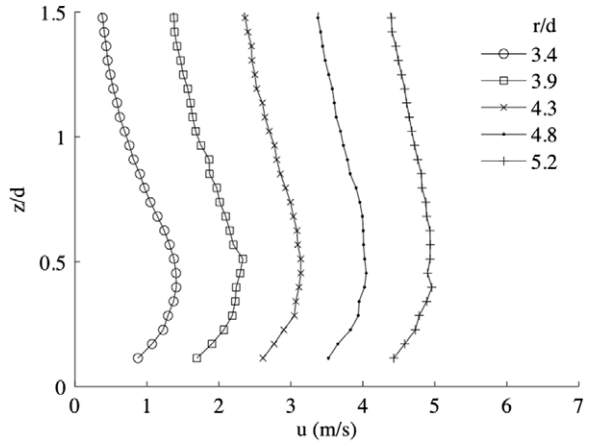

Fig. 9. The evolution of the mean velocity profiles in the radial direction. The velocities are displaced by 1 m/s successively starting at $r/d = 3.9$.

Measurements at wall normal distances less than 0.5 mm were not made.

Unlike free jets, the momentum flux in wall jets is not conserved on account of frictional losses at the walls. However, the loss of momentum due to friction is marginal even at radial distances (r/d) on the order of 100 [35]. To first order while neglecting the fluctuating components, the momentum flux was observed to decrease by no more that 2% over the region studied. This suggests that the jet is reasonably radial and that no significant pressure gradient as a result of the experimental setup was imposed upon the flow.

When the maximum velocity (u_m) of the wall jet is normalized by the synthetic jet mean velocity (U_o), and the inverse plotted against the non-dimensional radial distance (r/d), a straight line well represents the data (Fig. 10(a)). This suggests that the maximum velocity does indeed decay as $1/r$ and that the similarity exponent a is -1. Thus, in assuming a linear decay rate the variation of the centerline mean velocity with axial distance may be expressed as

$$\frac{U_o}{u_m} = A_u \left(\frac{r - r_{o,u}}{d} \right) \tag{13}$$

where, A_u is a scaled measure of the decay rate of the jet, and $r_{o,u}$ is the radial location of the virtual origin of U_o/u_m. The virtual origin is the apparent origin of the synthetic jet, and takes into account the fact that there is a developmental region in a real

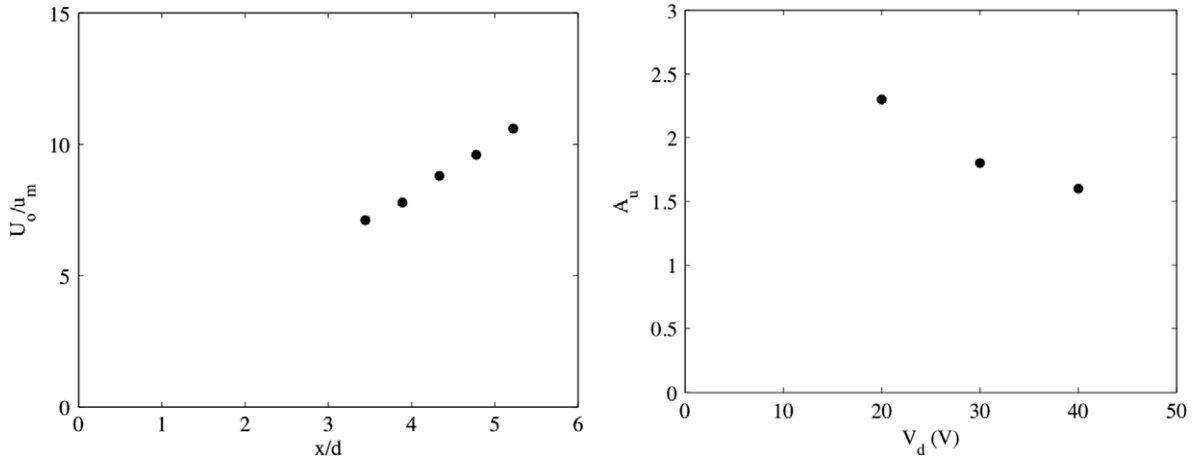

(a) The radial variation of the scaled inverse maximum velocity (U_o/u_m).

(b) Change in decay rate (A_u) with driving amplitude (V_d).

Fig. 10. Decay of the maximum centerline velocity.

synthetic jet that does not exhibit self-similarity. It is obtained from the intersection of the radial axis and the linear extrapolation of the maximum velocity. As shown in Fig. 10(b), an increase in driving amplitude (V_d) is observed to decrease the decay rate. Additionally it is also observed (not shown) that the distance between the virtual origin and the point of impact increases. From this study it was not possible to ascribe this variation in decay rate to either Reynolds number or stroke ratio exclusively, as a change in driving amplitude at a constant driving frequency impacts both the parameters simultaneously.

The growth of the jet is characterized by the growth of the half width ($z_{1/2}$). The half width is defined as the axial distance at which the velocity in the outer layer decreases to half the maximum velocity. Fig. 11(a) shows that the half width varies linearly with radial distance or that the similarity exponent b is 1. It is possible to express the spreading rate as

$$\frac{z_{1/2}}{d} = A_b \left(\frac{r - r_{o,b}}{d} \right), \tag{14}$$

where A_b is the scaled spreading rate of the jet, and $r_{0,b}$ is the location of the virtual origin based on the jet width. For the synthetic jet parameters considered both the spreading rate as seen in Fig. 11(b), and distance of the virtual origin from the stagnation point (not shown) increase with driving amplitude. Purely for comparative purposes, the spreading rate of a high Reynolds number continuous turbulent radial wall jet is cited to be 0.09 [12]. This variation in outer spreading rate with driving amplitude is much like that observed in free synthetic jets [27,36]. Thus, it seems to reason that increasing the driving amplitude enhances the mixing mechanism in the outer layer, resulting in the increased axial proliferation of the outer layer.

Fig. 12(a) presents the normalized mean velocity profiles at different radial locations downstream of the stagnation point for case 3. The velocity is scaled by the maximum velocity, while the axial distance from the wall is scaled by the outer half width. The mean velocity profiles are observed to collapse onto a single curve indicating that the velocity and length scales employed in the continuous jet-induced wall jets are appropriate for a synthetic wall jet as well. While the inner region does appear to collapse, it is known that this region does not scale precisely with the outer variables [12]. Due to the low local Reynolds number of the flow, measurements may have to be made closer to the wall to reveal this deviation.

Both the laminar and turbulent solutions (Section 2) are incapable of faithfully representing the scaled velocity profiles of the synthetic wall jet for the actuator conditions considered. With the turbulent nature of wall jet being evident, the laminar solution quite expectedly did not agree well with the experimental data. The deviation of the turbulent solution may be attributed as mention earlier to either the low local wall jet Reynolds number, or the effect of the high amplitude oscillations driving the flow. Further studies are required to assess the mixing mechanism in the synthetic wall jet so as to ascribe a reason for the deviation of the fully turbulent model from the experimental data. With the laminar and turbulent solutions failing to model the synthetic wall jet, Eq. (7) is resorted to. Eq. (7) is observed to agree well with the experimental profile when a fit to the data. The deviation towards the outer layer may be attributed to a secondary flow that develops due to both entrainment effects of the free jet, and confinement due to the surface of the actuator as is also observed in impinging continuous wall jets [37].

The profiles of the radial rms velocity when scaled appear to collapse onto a single curve (Fig. 12(b)). The profiles display a local maximum, but due to the lack of measurements closer to the wall a secondary maximum associated with the high shear stress near the wall is not captured [12]. However, the collapse of both the mean and rms profiles suggest that at the radial locations considered the jet broadly speaking has achieved self-similarity.

The power spectrum of the velocity time signal provides some additional insight into the happenings in the wall jet region. Fig. 13(a) presents the power spectra of the velocity signals in the inner and outer region of the wall jet at a fixed radial position. The signal is dominated by the driving frequency ($f_1 = 570$ Hz) and harmonics ($2f_1, 3f_1$) suggesting the continued influence of the coherent vortical structures initiated at the actuator, even upon impact and spreading. The frequency band below the driving frequency exhibits no subharmonics, leading to believe that in contrast to both forced and unforced continuous wall jets, vortex pairing between the vortical structures in the inner and outer layer [38] is not dominant in synthetic wall jets. Fig. 13(b) shows the spectra in the outer region of the jet at a fixed axial position at different radial locations. In progressively moving away from the stagnation point, the magnitude of the dominant frequency components decreases. However, the effect is marginal on account of the small range of the radial distance considered here. The additional peaks in the spectrum not associated with the actuator harmonics may be due to either the secondary vortical structures that emerge out of impact of the free jet with the wall [39], or due to the existence of skipping modes associated with the hot-wire that introduce superfluous higher frequencies not related to the content of the wall jet [1,40]. Summing up, the spectral data show

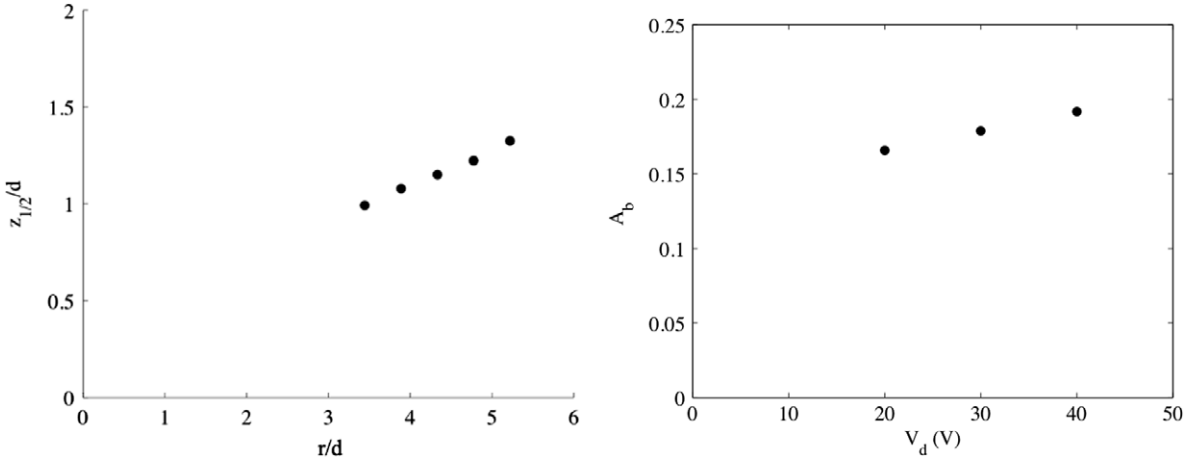

(a) The radial variation of the scaled half width ($z_{1/2}/d$).

(b) Change in spreading rate (A_b) with driving amplitude (V_d).

Fig. 11. Spreading of jet.

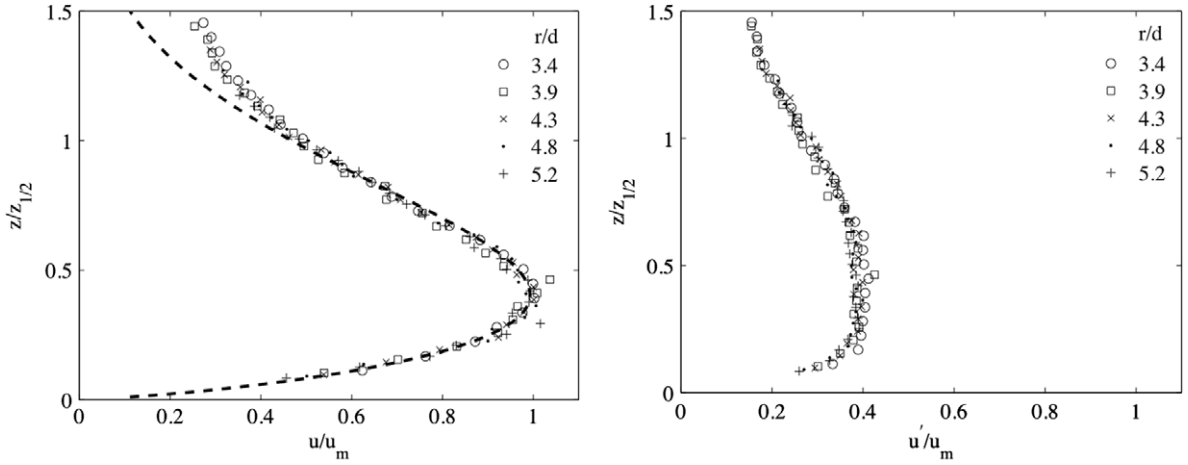

(a) Normalized radial mean velocity profiles exhibiting self-similar behavior. The analytical solution is represented by the dashed line.

(b) Normalized radial rms velocity profiles.

Fig. 12. Normalized velocity profiles.

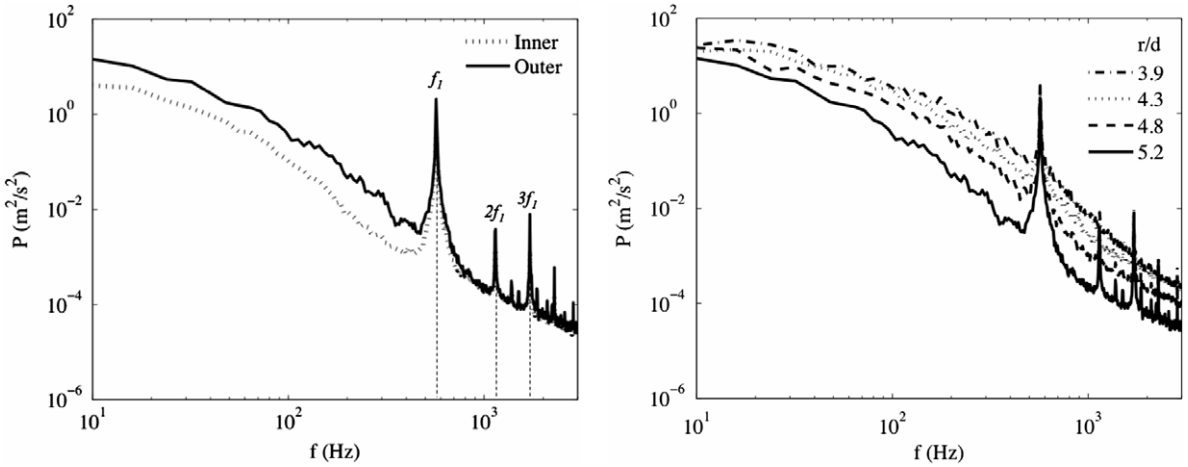

(a) Frequency spectra of the velocity signal in the inner ($z/d = 0.2$) and outer ($z/d = 0.8$) region of the wall jet, at a fixed radial distance ($r/d = 5.2$).

(b) Frequency spectra of the velocity signal in the outer region ($z/d = 0.8$) at different radial locations.

Fig. 13. Frequency spectra in the wall jet region.

that the fully pulsatile nature of the synthetic jet results in a mixing mechanism quite different from that present in continuous wall jets. Further work is required to provide a clearer description of the interaction of the vortical structures in the wall jet region.

5. Conclusion

Hot-wire anemometry was used to study the flow field of a wall jet induced by the impingement of a round synthetic jet normal to a wall. With previous work focusing on the impingement region of synthetic jets, the contribution of this study was to focus on the wall jet region. The synthetic wall jet showed similarities to continuous wall jets in (i) the linear growth of the outer layer, (ii) the inverse manner of decay of the maximum velocity, and (iii) the collapse of the mean and radial rms velocity profiles when normalized by the outer layer scaling. The spreading and decay rates however differ considerably from that of a high Reynolds number continuous wall jet. In contrast to continuous radial wall jets, the flow field of the synthetic wall jet was dominated by vortical structures associated with the actuator driving frequency, and harmonics connected with the interaction of the vortex structures. The effect of an increase in actuator driving amplitude at a fixed frequency was found to (i) increase the growth rate of the outer layer, and (ii) decrease the decay rate of the local velocity maximum. For the actuator conditions investigated, neither the classical laminar nor fully turbulent analytical solutions to continuous wall jets were able to model the synthetic wall jets. However, a fully empirical form did indeed accommodate the transitional and unsteady nature of the synthetic wall jet. It is speculated that if a higher Reynolds number flow was achieved, that the turbulent solution will model the flow through the use of a single empirically determined parameter. While this study does provide a preliminary description of the flow field of a synthetic wall jet, further understanding could be derived from (i) the independent variation of the stroke ratio and Reynolds number to assess their individual effects, and (ii) the extension of the actuator parameters to determine the applicability of a fully turbulent wall jet model to synthetic wall jets.

Acknowledgement

The authors would like to acknowledge partial support from the Air Force Office of Scientific Research.

References

[1] B. Smith, A. Glezer, The formation and evolution of synthetic jets, Phys. Fluids 10 (9) (1998) 2281–2297.
[2] A. Glezer, M. Amitay, Synthetic jets, Annu. Rev. Fluid Mech. 34 (2002) 503–529.
[3] D. Kercher, J. Lee, O. Brand, M. Allen, A. Glezer, Microjet cooling devices for thermal management of electronics, IEEE Trans. Compon. Packag. Technol. 26 (2) (2003) 359–366.
[4] J. Garg, M. Arik, S. Weaver, T. Wetzel, S. Saddoughi, Meso scale pulsating jets for electronics cooling, J. Electron. Packag. 127 (4) (2005) 503–511.
[5] R. Mahalingam, N. Rumigny, A. Glezer, Thermal management using synthetic jet ejectors, IEEE Trans. Compon. Packag. Technol. 27 (3) (2004) 439–444.
[6] R. Mahalingam, A. Glezer, Design and thermal characteristics of a synthetic jet ejector heat sink, J. Electron. Packag. 127 (2) (2005) 172–177.
[7] A. Pavlova, M. Amitay, Electronic cooling using synthetic jet impingement, J. Heat Transfer 128 (9) (2006) 897–907.
[8] Y. Utturkar, M. Arik, C.E. Seeley, M. Gursoy, An experimental and computational heat transfer study of pulsating jets, J. Heat Transfer 130 (6) (2008).
[9] T.S. O'Donovan, D.B. Murray, Jet impingement heat transfer—part I: mean and root-mean-square heat transfer and velocity distributions, Int. J. Heat Mass Transfer 50 (17–18) (2007) 3291–3301.
[10] T.S. O'Donovan, D.B. Murray, Jet impingement heat transfer—part II: a temporal investigation of heat transfer and local fluid velocities, Int. J. Heat Mass Transfer 50 (17–18) (2007) 3302–3314.
[11] C.P. Donaldson, R.S. Snedeker, A study of free jet impingement. 1. Mean properties of free and impinging jets, J. Fluid Mech. 45 (Part 2) (1971) 281–319.
[12] B.E. Launder, W. Rodi, The turbulent wall jet—measurements and modeling, Annu. Rev. Fluid Mech. 15 (1983) 429–459.
[13] I. Wygnanski, Y. Katz, E. Horev, On the applicability of various scaling laws to the turbulent wall jet, J. Fluid Mech. 234 (1992) 669–690.
[14] W. George, H. Abrahamsson, J. Eriksson, R. Karlsson, L. Lofdahl, M. Wosnik, A similarity theory for the turbulent plane wall jet without external stream, J. Fluid Mech. 425 (2000) 367–411.
[15] N. Tetervin, Laminar flow of a slightly viscous incompressible fluid that issues from a slit and passes over a flat plate, NACA TN 1644, 1948, p. 40.
[16] M.B. Glauert, The wall jet, J. Fluid Mech. 1 (6) (1956) 625–643.
[17] R. Bajura, A. Szewczyk, Experimental investigation of a laminar two-dimensional plane wall jet, Phys. Fluids 13 (7) (1970) 1653–1664.
[18] P. Bakke, An experimental investigation of a wall jet, J. Fluid Mech. 2 (5) (1957) 467–472.
[19] M. Poreh, Y. Tsuri, J. Cermak, Investigation of turbulent radial wall jet, American Society of Mechanical Engineers. Trans. ASME J. Appl. Mech. 34 (2) (1967) 457–463.
[20] D. Quintana, M. Amitay, A. Ortega, I. Wygnanski, Heat transfer in the forced laminar wall jet, J. Heat Transfer 119 (3) (1997) 451–459.
[21] J. Seidel, H. Fasel, Numerical investigations of heat transfer mechanisms in the forced laminar wall jet, J. Fluid Mech. 442 (2001) 191–215.
[22] Y. Katz, E. Horev, I. Wygnanski, The forced turbulent wall jet, J. Fluid Mech. 242 (1992) 577–609.
[23] M. Schober, H. Fernholz, Turbulence control in wall jets, Eur. J. Mech. B Fluids 19 (4) (2000) 503–528.
[24] A. Glezer, The formation of vortex rings, Phys. Fluids 31 (12) (1988) 3532–3542.
[25] J. Vejrazka, J. Tihon, P. Marty, V. Sobolik, Effect of an external excitation on the flow structure in a circular impinging jet, Phys. Fluids 17 (2005) 105102–1–14.
[26] Y. Utturkar, R. Holman, R. Mittal, B. Carroll, M. Sheplak, L. Cattafesta, A jet formation criterion for synthetic jet actuators, AIAA Paper 2003-636.
[27] J. Shuster, D. Smith, Experimental study of the formation and scaling of a round synthetic jet, Phys. Fluids 19 (4) (2007) 45109–1–21.
[28] G. Krishnan, K. Mohseni, Axisymmetric synthetic jets: an experimental and theoretical examination, AIAA J. 47 (10) (2009) 2273–2283.
[29] G. Krishnan, K. Mohseni, An experimental and analytical investigation of rectangular synthetic jets, ASME J. Fluids Eng. 131 (12) (2009), doi:10.1115/1.4000422.
[30] X. Xia, K. Mohseni, Modeling and experimental investigation of synthetic jets in cross- flow, AIAA Paper 2010-0106, in: 48th AIAA Aerospace Sciences Meeting Including the New Horizons Forum and Aerospace Exposition, Orlando, FL, January 4–7, 2010.
[31] G. Wood, K. Kwok, N. Motteram, D. Fletcher, Physical and numerical modelling of thunderstorm downbursts, J. Wind Eng. Ind. Aerodyn. 89 (6) (2001) 535–552.
[32] S. Timoshenko, Theory of Plates and Shells, McGraw-Hill, 1999.
[33] B.L. Smith, G. Swift, Synthetic jets at larger reynolds number and comparison to continuous jets, AIAA Paper 2001-3030.
[34] A. Johnstone, M. Uddin, A. Pollard, Calibration of hot-wire probes using non-uniform mean velocity profiles, Exp. Fluids 39 (3) (2005) 525–532.
[35] B. Launder, W. Rodi, The turbulent wall jet, Prog. Aerosp. Sci. 19 (2–4) (1981) 81–128.
[36] G. Krishnan, K. Mohseni, On the modelling of a synthetic jet as a spherical jet, FEDSM Paper 2007, Part B, 2007, pp. 1545–1552.
[37] M. Fairweather, G. Hargrave, Experimental investigation of an axisymmetric, impinging turbulent jet. 1. Velocity field, Experiments in Fluids 33 (3) (2002) 464–471.
[38] R. Bajura, M. Catalano, Transition in a 2-dimensional plane wall jet, J. Fluid Mech. 70 (4) (1975) 773–799.
[39] N. Didden, C.M. Ho, Unsteady separation in a boundary-layer produced by an impinging jet, J. Fluid Mech. 160 (1985) 235–256.
[40] S. Mallinson, J. Reizes, G. Hong, P. Westbury, Analysis of hot-wire anernometry data obtained in a synthetic jet flow, Exp. Thermal Fluid Sci. 28 (4) (2004) 265–272.